

# Dielectric Relaxor Evolution and Frequency-Insensitive Giant Strains in $(\text{Bi}_{0.5}\text{Na}_{0.5})\text{TiO}_3$ -Modified $\text{Bi}(\text{Mg}_{0.5}\text{Ti}_{0.5})\text{O}_3$ - $\text{PbTiO}_3$ Ferroelectric Ceramics

Wanli Zhao,<sup>‡</sup> Ruzhong Zuo,<sup>‡,†</sup> Donggeng Zheng,<sup>‡</sup> and Longtu Li<sup>§</sup>

<sup>‡</sup>Institute of Electro Ceramics & Devices, School of Materials Science and Engineering, Hefei University of Technology, Hefei 230009, China

<sup>§</sup>State Key Laboratory of New Ceramics and Fine Processing, Department of Materials, Science and Engineering, Tsinghua University, Beijing 100084, China

The  $0.45\text{Bi}(\text{Mg}_{0.5}\text{Ti}_{0.5})\text{O}_3$ - $(0.55 - x)\text{PbTiO}_3$ - $x(\text{Bi}_{0.5}\text{Na}_{0.5})\text{TiO}_3$  (BMT-PT- $x$ BNT) ternary solid solution ceramics were prepared via a conventional solid-state reaction method; the evolution of dielectric relaxor behavior and the electrostrain features were investigated. The XRD and dielectric measurements showed that all studied compositions own a single pseudocubic perovskite structure and undergo a diffuse-to-relaxor phase transition owing to the evolution of the domain from a frozen state to a dynamic state. The formation of the above dielectric relaxor behavior was further confirmed by a couple of measurements such as polarization loops, polarization current density curves, as well as bipolar strain loops. A large strain value of  $\sim 0.41\%$  at a driving field of 7 kV/mm (normalized strain  $d_{33}^*$  of  $\sim 590$  pm/V) was obtained at room temperature for the composition with  $x = 0.32$ , which is located near the boundary between ergodic and nonergodic relaxor. Moreover, this electric field-induced large strain was found to own a frequency-insensitive characteristic.

## I. Introduction

PIEZOELECTRIC ceramics have been widely used in various applications such as sensors and actuators which are mainly dominated by lead-based materials during the past decades due to their excellent piezoelectric properties.<sup>1–3</sup> As far as the application of piezoelectric actuators is concerned, the electric field-induced strain property is one of the most important parameters. It is known that the antiferroelectric order can obviously enhance the strain level and a large strain value of  $\sim 0.4\%–0.5\%$  was usually reported in antiferroelectric ceramics owing to the field-induced antiferroelectric-to-ferroelectric phase transition.<sup>4</sup>

Aside from the lead-based materials, Bi-based perovskite-structured solid solutions of  $\text{BiMeO}_3$ - $\text{PbTiO}_3$  have recently attracted lots of attention due to their high Curie temperature ( $T_c$ ), in which  $Me$  consists of cations with an average 3+ valence.<sup>5–10</sup> It was argued that the high  $T_c$  value benefits from the enhanced spontaneous polarization due to a similar “lone-pair”  $6s^2$  electronic configuration of  $\text{Bi}^{3+}$  to  $\text{Pb}^{2+}$  and a strong coupling in the polarization between  $A$ -site and  $B$ -site cations.<sup>11</sup> Among the various Bi-based materials,  $\text{Bi}(\text{Mg}_{0.5}\text{Ti}_{0.5})\text{O}_3$ - $\text{PbTiO}_3$  (BMT-PT) was considered as one of the most promising candidates for high-temperature applications due to its high  $T_c$ , acceptable piezoelectric performance, and a relatively low cost.<sup>5–8</sup> Very recently, BMT-PT-based

ternary systems have been studied owing to their specific structures and electrical properties.<sup>12–17</sup> More importantly, a comparable strain value (up to  $\sim 0.4\%$ ) was also obtained under high external electric fields in some of these ternary systems through the substitution of some zirconates.<sup>16,17</sup> This large strain was initially proposed to be related to the field-induced antiferroelectric relaxor-to-ferroelectric phase transformation due to the pinched polarization versus electric field ( $P$ - $E$ ) loops.<sup>16,17</sup> The antiferroelectric feature was considered to originate from BMT with an analogous structure to  $\text{PbZrO}_3$ .<sup>18</sup> However, no direct evidence manifested the antiferroelectric order in these systems other than the  $P$ - $E$  measurements. Later on, the achievement of the giant strain in BMT-based system was found to be accompanied by the evolution of a relaxor behavior owing to a change in the dynamics of the polar nanoregions (PNRs), while the induced relaxors own a ferroelectric nature.<sup>19</sup> Despite of the different explanations about the formation of giant strains, it would be noted that the achievement of a relaxor property might play an important role in these BMT-based large strain systems.<sup>16,17,19</sup> The same situation has also been observed in  $(\text{Bi}_{0.5}\text{Na}_{0.5})\text{TiO}_3$  (BNT)-based systems substituted by components like  $(\text{Na}_{0.5}\text{K}_{0.5})\text{NbO}_3$  (NKN),  $\text{SrTiO}_3$ ,  $\text{Zr}^{4+}$ , and so on.<sup>20–24</sup> The achievement of the large strain in BNT-based ceramics was identified as a consequence of a field-induced phase transition between a nonpolar phase (ergodic relaxor) and ferroelectric phase.<sup>21,22,24</sup>

It is believed that the relaxor behavior can be usually observed in complex perovskites and the disordered distribution of different ions at one or more equivalent crystallographic sites is an essential characteristic of relaxors. This disorder distribution induces local random fields which are responsible for the growth of PNRs.<sup>19,25–27</sup> The presence of these PNRs and correlations among them should be closely associated with the evolution of relaxor behavior. With increasing the size of the PNRs, the relaxors could transform into a normal ferroelectric and sometimes into an intermediate phase with a diffuse phase transition, but without frequency dispersion between relaxor and normal ferroelectrics.<sup>28</sup> It was argued that the distinction between frequency independent diffuse phase transition and frequency-dependent relaxor-like behaviors is due to the different sizes of the PNRs.<sup>29</sup> Interestingly, diffuse phase transition has been reported in BMT-PT compositions and these compositions were characterized by polar domains of  $\sim 50$  nm with a frozen-in polarization (static) state,<sup>5</sup> which are much larger than the PNRs in canonical  $\text{Pb}(\text{Mg}_{1/3}\text{Nb}_{2/3})\text{O}_3$ .

BNT was reported to be a typical relaxor ferroelectric of the perovskite structure with  $A$ -site being equally shared by two different cations ( $\text{Bi}^{3+}$  and  $\text{Na}^+$ ).<sup>30–32</sup> The substitution of BNT in BMT-PT can be then expected to increase the disordered degree of BMT-PT solid solutions, inducing a diffuse-to-relaxor phase transformation. The purpose of this

S. Zhang—contributing editor

study was thus to explore the effect of the BNT substitution on the dielectric properties of diffuse-type BMT–PT binary system and the accompanying electric field-induced electrostrains by using a fixed BMT content of 45% and then substituting BNT for PT. These studied compositions would be expected to lie on the rhombohedral side of the morphotropic phase boundary of BMT–PT–BNT ternary system.

## II. Experimental Procedure

The conventional mixed-oxide route was adopted to prepare the 0.45BMT–(0.55– $x$ )PT– $x$ BNT (abbreviated as BMT–PT– $x$ BNT,  $x = 0.27$ – $0.34$ ) ceramics. The high-purity (>99%)  $\text{Bi}_2\text{O}_3$ ,  $\text{TiO}_2$ ,  $\text{Na}_2\text{CO}_3$ ,  $\text{PbO}$ , and  $(\text{MgCO}_3)_4\text{Mg}(\text{OH})_2 \cdot 5\text{H}_2\text{O}$  were used as raw materials. The powder mixture was ball-milled in ethanol using  $\text{Y}_2\text{O}_3$ -stabilized zirconia balls for 6 h. The calcination was performed twice in a sealed  $\text{Al}_2\text{O}_3$  crucible at  $850^\circ\text{C}$  for 2 h. The calcined powders were crushed and ball-milled in ethanol again for 8 h. The compacted sample disks were sintered in air in sealed crucibles at  $1060^\circ\text{C}$ – $1100^\circ\text{C}$  for 2 h.

The relative densities were evaluated by the Archimedes method. A relative density of >97% can be achieved for all the studied samples at their optimal sintering temperatures. The crystal structure was examined by an XRD (D/Max-RB; Rigaku, Tokyo, Japan) using  $\text{CuK}\alpha$  radiation. The microstructure was observed using a scanning electron microscope (SEM, JEOL JSM-6490LV; Tokyo, Japan). Two major surfaces of the pellets were covered with a thin layer of silver paste and fired at  $550^\circ\text{C}$  for 30 min. The samples were poled at a dc field of 6–7 kV/mm at room temperature for 5 min in silicone oil. The quasi-static piezoelectric constant ( $d_{33}$ ) was measured by using a Belincourt meter (YE2730A; Sino-cera, Yangzhou, China). Dielectric properties were measured as a function of temperature and frequency by an LCR meter (Agilent E4980A; Santa Clara, CA) in the frequency range 1 kHz–1 MHz in the temperature range  $25^\circ\text{C}$ – $500^\circ\text{C}$ . The polarization versus electric field loops ( $P$ – $E$ ) and electric field-induced strain ( $S$ – $E$ ) curves were measured at room temperature by using a ferroelectric measuring system (Precision multiferroelectric, Radiant Technologies Inc., Albuquerque, NM) with an accessory laser interferometer vibrometer (AE SP-S 120E; SIOS Meßtechnik, GmbH, Ilmenau, Germany). All the electrical measurements were repeated for several times by using 3–4 samples for each composition and only a very small difference between these measurement results could be detected, indicating that the experimental data could be well repeated.

## III. Results and Discussion

Figure 1 shows the XRD patterns of the BMT–PT– $x$ BNT powders by crushing the samples densified at  $1080^\circ\text{C}$ . The results revealed a single perovskite structure without any apparent secondary phases for all the studied compositions, as can be seen in Fig. 1(a). The locally magnified (111) and (200) peaks, which are the characteristic peaks for rhombohedral and tetragonal phases, respectively, indicate no obvious peak splitting, as shown in Figs. 1(b) and (c). Moreover, only single diffraction peaks were detected up to  $80^\circ$  (peaks are too weak to be detected as diffraction angle is higher than  $80^\circ$  for our current instrument condition). Sharp and narrow peak profiles suggest a cubic perovskite structure with a negligible noncubic distortion for all compositions. Similar results have also been observed in the XRD analysis of the BMT–PT binary system with a low PT content.<sup>6</sup> However, it should be noted that a completely cubic symmetry would be inconsistent with all the macroscopic properties reported in this system. Thus, it would be reasonable to assume that the symmetry of the materials should be lower than cubic. That is to say a pseudocubic distortion probably exists in a very fine scale beyond the detection limit of the

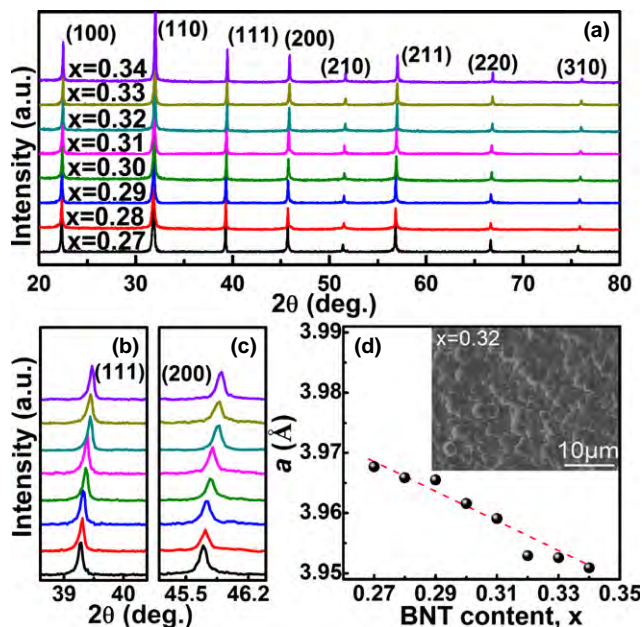


Fig. 1. (a) Room-temperature powder XRD patterns of BMT–PT– $x$ BNT ceramics, the locally magnified (b) (111) and (c) (200) diffraction peaks and (d) lattice constant  $a$  as a function of the BNT content. The inset shows the SEM picture for  $x = 0.32$  sample.

currently employed XRD technique. On the other hand, the (111) and (200) diffraction peaks reveal a slight shift to higher diffraction angles with increasing the BNT content, indicating that there is a slight lattice contraction. This is probably due to relatively small ionic radii of  $\text{Bi}^{3+}$  and  $\text{Na}^+$  compared with  $\text{Pb}^{2+}$  at the  $A$ -site ( $CN = 12$ ,  $R_{\text{Na}} = 1.39 \text{ \AA} < R_{\text{Bi}} = 1.45 \text{ \AA} < R_{\text{Pb}} = 1.49 \text{ \AA}$ ).<sup>33</sup> The corresponding lattice parameter  $a$  for samples with different BNT contents was calculated based on a pseudocubic structure, as shown in Fig. 1(d). It is obvious that the lattice parameter  $a$  decreased slightly with increasing the BNT content. Moreover, the microstructure of the studied samples was examined by SEM. A representative result for the  $x = 0.32$  sample sintered at  $1080^\circ\text{C}$  was given, as shown in the inset of Fig. 1(d). The SEM examination confirms the high-density and well-developed grains with a uniform grain size of 2–3  $\mu\text{m}$ . Moreover, we did not detect any obvious changes in the grain size and morphology with changing BNT content probably due to a relatively narrow composition range.

The dielectric property of this system was measured as functions of temperature and frequency, as shown in Figs. 2(a–h). The measuring frequency ranges from 1 kHz to 1 MHz and the arrow indicates the direction of increasing frequency. First, the temperature at the dielectric maximum ( $T_m$ ) decreased slightly with increasing the BNT content, probably owing to the relatively low Curie temperature of BNT compared with PT. Second, it is obvious that the studied compositions exhibited the dielectric diffuse-relaxor phase transformation. Third, the frequency dependence of  $T_m$  increased with increasing the BNT content, meaning that the substitution of BNT enhanced the degree of the dielectric relaxation. The  $\gamma$  value, which was calculated from the modified Curie–Weiss law, was considered as the degree of relaxation ranging between 1 for a normal ferroelectric and 2 for an ideal relaxor ferroelectric,<sup>34</sup> and  $\Delta T_{\text{relax}}$ , defined as  $\Delta T_{\text{relax}} = T_{1\text{MHz}} - T_{1\text{kHz}}$ ,<sup>35</sup> was also plotted as a function of the BNT content, as shown in Fig. 2(i). It is clear that both  $\gamma$  and  $\Delta T_{\text{relax}}$  values increase monotonously with increasing the BNT content. The  $x = 0.27$  sample owns  $\gamma = 1.63$ , but  $\Delta T_{\text{relax}} = 0$ , indicating that this composition is diffuse type but in the absence of frequency dispersion. As known, the disordered distribution of different ions would induce the

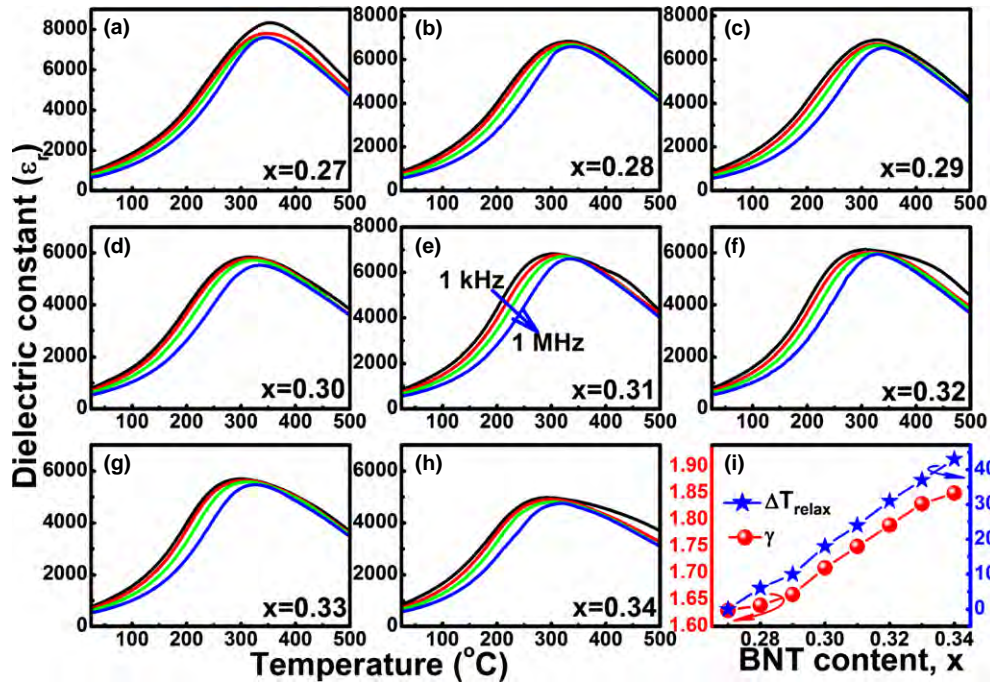


Fig. 2. (a–h) Temperature and frequency dependence of dielectric constant for BMT–PT–xBNT ceramics and (i) the corresponding change in  $\gamma$  and  $\Delta T_{\text{relax}}$  as a function of the BNT content.

formation of random local fields owing to the local charge imbalance or different ionic sizes.<sup>19,25–27,36–38</sup> The evolution of the dielectric relaxor behavior in this system could be ascribed to the change in the random local field. The characteristic of the diffuse-type phase transition means that the induced random local field in the  $x = 0.27$  sample would be not strong enough to disrupt the long-range polar correlations, such that the PNRs cannot be generated or the generated PNRs are too large in size.<sup>19,38</sup> Similar phenomenon has been observed in BMT–PT binary system and Randall *et al.*<sup>5</sup> demonstrated that the domain structure of rhombohedral BMT–PT ceramics consists of  $\sim 50$ -nm-sized polar microdomains, which are much larger than the PNRs in canonical  $\text{Pb}(\text{Mg}_{1/3}\text{Nb}_{2/3})\text{O}_3$ . Therefore, the structural and/or chemical disorder might exist, but its domains are frozen and only can be switched under a sufficiently large electric field.<sup>5,19</sup> The diffuse-to-relaxor phase transformation behavior with increasing the BNT content indicates that the random local fields gradually increased in this system and the long-range polar correlations tended to be broken. Based on the above analysis, a gradual increase in the dynamics of PNRs in this system would be expected as well as a decrease in size of PNRs with increasing the BNT content. In combination with the analysis of the above XRD results, the microstructure of the BMT–PT–xBNT ternary composition can be considered to consist of PNRs with a noncubic distortion embedded into a cubic matrix in which the symmetry remains unchanged.<sup>39,40</sup> The average structure could be more properly described as a pseudocubic phase.

Figures 3(a)–(h) depicts the room-temperature  $P$ - $E$  loops for all compositions as well as the corresponding current density loops ( $J$ - $E$ ), which provide a more detailed picture of the switching processes. The corresponding change tendency of the maximum polarization ( $P_{\text{max}}$ ), remanent polarization ( $P_r$ ), and coercive field ( $E_c$ ) was also summarized in Fig. 3(i). It is obvious that as  $x > 0.31$ , slim and unsaturated  $P$ - $E$  loops were obtained with a relatively low  $P_r$  value. The corresponding  $E_c$  remained in a low value and did not change much. At the same time, no obvious current peaks could be observed but only a broad and flat current platform was obtained. All these features are typical for ergodic relaxors. In contrast, saturated and square  $P$ - $E$  loops were observed

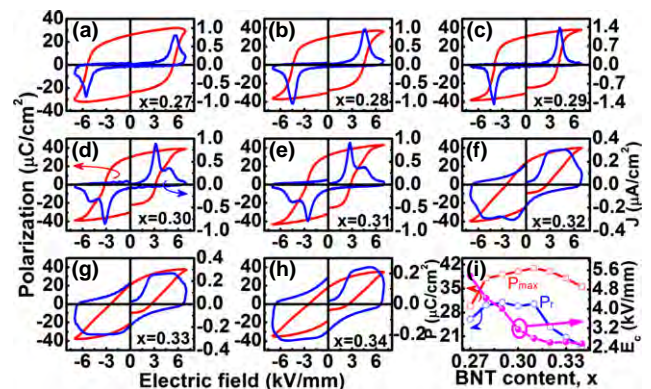


Fig. 3. (a–h)  $P$ - $E$  hysteresis loops and associated  $J$ - $E$  curves of BMT–PT–xBNT ceramics measured at a frequency of 1 Hz and (i) the corresponding change in  $P_{\text{max}}$ ,  $P_r$ , and  $E_c$  as a function of the BNT content.

for samples with  $0.28 \leq x \leq 0.29$ . Simultaneously, a single sharp polarization current peak, which was ascribed to the domain switching, could be observed at  $E = E_c$ . This is typical for materials with a long-range ferroelectric ordering. In particular, slightly pinched  $P$ - $E$  loops were observed for compositions with  $0.30 \leq x \leq 0.31$  and an additional current peak was observed. This indicates that the long-range polar correlations was disturbed compared with the  $0.28 \leq x \leq 0.29$  samples. However, it is noted that the  $P_r$  and  $P_{\text{max}}$  did not change much in the composition range of  $0.28 \leq x \leq 0.31$ , although a monotonous decrease in the  $E_c$  value was observed with increasing the BNT content. This demonstrated that, in spite of the disruption of the polar correlations, the long-range polar correlations could be still obtained under the application of a strong enough external field (e.g. 7 kV/mm in this study), and most of the induced long-range polar correlations could be maintained after removal of the electric field. By comparison, a comparable  $P_{\text{max}}$  value could be obtained as  $x > 0.31$ , yet it could not be maintained after the external field was released, resulting in a lower  $P_r$  value. This is also typical feature for ergodic

relaxors. All these differences could be ascribed to the variation in the dynamics of PNRs as discussed above. With an increase in the BNT content, the dynamics of PNRs increases, which would tend to destroy the long-range polar correlations. This should also be responsible for the decrease in the  $E_c$  value. As  $x = 0.27$ , a rounded  $P$ - $E$  loop was obtained with a significant decrease in both  $P_{\max}$  and  $P_r$ . As discussed above, this composition possessed a diffuse-type phase transition around  $T_m$  and the domains in this composition are frozen, such that the current field strength is not strong enough to induce a full poling state for this sample.

The electrostrain property measured at a frequency of 1 Hz as a function of bipolar electric field at room temperature for BMT-PT- $x$ BNT ceramics is shown in Fig. 4(a), which would be an effective method to verify the composition modulated dielectric relaxor as discussed above. As can be seen, sprout-shaped strain hysteresis loops were obtained for samples with  $x \geq 0.32$  with the absence of the negative strain [ $S_{\text{neg}}$ , denoted by the difference between the minimum strain and the strain at zero electric field during bipolar cycles, see the inset of Fig. 4(a)]. This is a typical performance for ergodic relaxor materials.<sup>21–24</sup> For samples with  $x < 0.32$ , the sprout-shaped strain hysteresis loops changed into butterfly-shaped ones. Meantime, a gradual increase in the negative strain was observed. According to the above analysis on the dielectric and  $P$ - $E$  measurements, it could be basically determined that fresh samples with  $0.28 \leq x \leq 0.29$  would exist in a nonergodic relaxor state at room temperature because the field-induced nonergodic-to-ferroelectric phase transition is known to be irreversible. Therefore, the fresh samples with  $0.30 \leq x \leq 0.31$  would exist in a transitional state with the coexistence of ergodic and nonergodic phases and such a phase coexistence would be responsible for the presence of the two separated current peaks (see Fig. 3).<sup>41</sup> The positive strain [ $S_{\text{pos}}$ , denoted by the difference

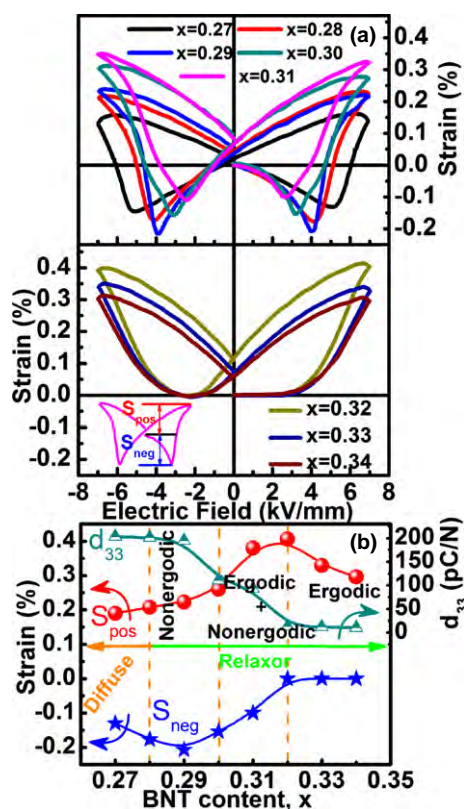


Fig. 4. (a) Bipolar  $S$ - $E$  loops for BMT-PT- $x$ BNT ceramics measured at room temperature at a frequency of 1 Hz and (b) the variation in  $S_{\text{pos}}$  and  $S_{\text{neg}}$  with the BNT content as well as the quasi-static  $d_{33}$  values.

between the maximum strain and the strain at zero electric field during bipolar cycles, also see the inset of Fig. 4(a)] and  $S_{\text{neg}}$  as a function of the BNT content was summarized in Fig. 4(b) where different phase zones were roughly indicated. At the same time, the change tendency of the corresponding quasi-static  $d_{33}$  was also listed in Fig. 4(b). On the one hand, it is apparent that the achievement of the large electric field-induced strain was accompanied by a drastic decrease in the  $S_{\text{neg}}$  value and similar phenomena have also been observed in other Bi-containing perovskite-structured ferroelectrics.<sup>16,17,19,21–24</sup> Moreover, it is apparent that the absolute value of  $S_{\text{neg}}$  first increased for  $0.27 < x < 0.29$  and reached the maximum at  $x = 0.29$ . It is proposed that the increase in  $S_{\text{neg}}$  should originate from the transformation of frozen domains into the nonergodic phase with an increased contribution to  $S_{\text{neg}}$  and a complete nonergodic state was obtained at  $x = 0.29$  (for the fresh sample). Thus, the sample with  $x = 0.28$  would have a coexistence of short-range polar ordering state (nonergodic state) and frozen-in domain state. The following decrease in  $S_{\text{neg}}$  with a further increase in the BNT content ( $0.29 < x < 0.32$ ) should originate from the decrease in the nonergodic phase and finally the transformation of the nonergodic phase into the ergodic phase. On the other hand, the quasi-static  $d_{33}$  decreased with increasing the BNT content, and near-zero  $d_{33}$  values were detected for samples with  $x > 0.31$ , which could also confirm the ergodicity in samples with high BNT contents.

Figure 5 shows the unipolar strain loops of BMT-PT- $x$ BNT ceramics measured at room temperature and all the strain data were obtained from nonfirst cycles. A large strain of 0.41% and corresponding  $d_{33}^*$  ( $d_{33}^* = S_{\text{max}}/E_{\text{max}}$ , see the upper inset of Fig. 5) of 590 pm/V were obtained for the sample with  $x = 0.32$  at an applied electric field of 7 kV/mm. A decrease in the strain value was observed at both sides of the  $x = 0.32$  sample. In addition, it is clear that samples with  $x \leq 0.29$  exhibit an almost linear strain response with small hysteresis, which is typical for ferroelectric materials, indicating a large amount of intrinsic contributions to the strain response. The intrinsic contribution is mainly referred to the (converse) piezoelectric effect, i.e., the variation in the lattice distortion, which is proportional to the applied electric field. For samples with higher BNT contents ( $x > 0.30$ ), the strain

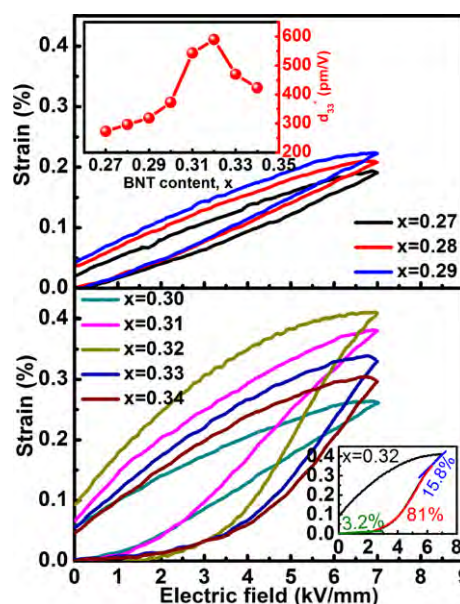


Fig. 5. Unipolar  $S$ - $E$  loops for BMT-PT- $x$ BNT ceramics measured at room temperature at a frequency of 1 Hz. The upper inset shows the variation in  $d_{33}^*$  with the BNT content, and the lower inset schematically indicates the different contributions to the unipolar strain curve of the  $x = 0.32$  sample.

curves show an  $S$ -shape curve with a pronounced hysteresis, indicating a different origin of the electric field-induced strain. Considering the fact that comparable  $P_{\max}$  values were acquired for these samples, it could be proposed that the free energy of the field-induced long-range ferroelectric order in these compositions appears competitive with that of the ergodic phase at zero electric field so that the long-range polar correlations can be easily induced by an external electric field. This field-induced reversible ergodic relaxor-ferroelectric phase transition was considered to be responsible for the observed field-induced giant strain.<sup>21,22,24</sup> However, the electrostriction effect as well as the piezoelectric effect could not be completely excluded in this system. Both effects have a contribution to the achievement of the large strain value. As can be seen from the lower inset of Fig. 5, a relatively small but linear strain was observed under low electric fields ( $\sim 2$  kV/mm), which may correspond to a low field piezoelectric effect as well as the electrostriction effect, making a contribution of about  $\sim 3.2\%$  of the total strain values. After this, the strain curve shows an  $S$ -shape change with a pronounced hysteresis until  $\sim 6$  kV/mm. This period was ascribed to the effect of the reversible ergodic relaxor-ferroelectric phase transition, which made a dominant contribution to the final strain ( $\sim 81\%$ ). At the end, the sample should be in a complete long-range ferroelectric state. The remaining  $\sim 15.8\%$  strains might be due to the further switching of ferroelectric domains as the electric field increased. Nevertheless, it should be noted that the obtained strain curves were not closed. An apparent remanent strain ( $S_r$ ) as observed in Fig. 5 would make one be confused with whether the achieved giant strain can be applied or not. Actually, all the strain loops were recorded from nonfirst cycles and could be well repeated in each independent testing process. The appearance of  $S_r$  in this work could be ascribed to the hysteresis effect of the ergodic PNRs' back switching as the applied electric field comes back to zero, although this process is definitely reversible. So, the observed  $S_r$  was not a stable one in these ergodic compositions and would disappear after removal of the electric field. It was called as the  $S_{\text{obs}}$ . This is different from that observed in the first cycle of materials in a nonergodic state or normal ferroelectric state (the observed  $S_r$  was a stable one and would not disappear after removal of the electric field). Here, the appearance of the apparent remanent strains ( $S_{\text{obs}}$ ) in currently studied compositions would have no influence on the calculation of the normalized strain  $d_{33}^*$ .

Figures 6(a) and (b) show the frequency-dependent unipolar strain loops, the maximum strains, and the normalized

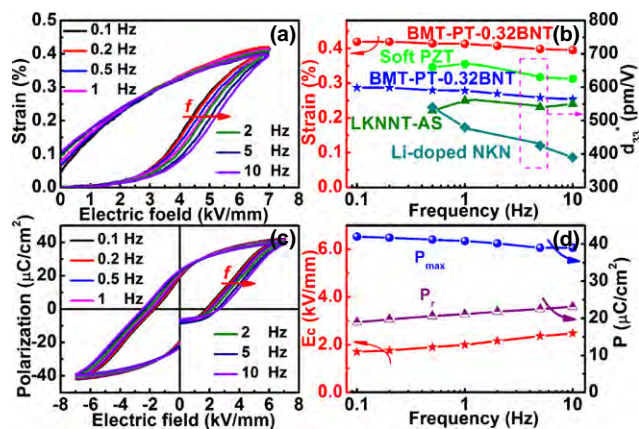


Fig. 6. (a) Unipolar  $S$ - $E$  loops for the  $x = 0.32$  sample at 7 kV/mm as a function of frequency, (b) the maximum strain against frequency of the  $x = 0.32$  sample, and a comparison of its  $d_{33}^*$  value against frequency with that of other ferroelectric ceramics, (c) frequency-dependent  $P$ - $E$  loops, and (d) the corresponding change in  $P_{\max}$ ,  $P_r$ , and  $E_c$  as a function of frequency for the  $x = 0.32$  sample.

strain  $d_{33}^*$  against frequency of BMT-PT-0.32BNT ceramic at 7 kV/mm. The maximum  $d_{33}^*$  values against frequency for some other ferroelectric ceramics<sup>42</sup> were also plotted in Fig. 6(b) for comparison. The frequency-dependent  $P$ - $E$  hysteresis loops as well as the corresponding change in  $P_{\max}$ ,  $P_r$ , and  $E_c$  with frequency are shown in Figs. 6(c) and (d). It is obvious that the  $x = 0.32$  sample exhibited a frequency-insensitive giant strain behavior. Its value ranges only between 0.40% and 0.42% within the studied frequency range 0.1–10 Hz. The  $x = 0.32$  sample in this study shows comparable  $d_{33}^*$  values with the reported materials like LKNNT-AS and soft PZT and more insensitive strains against frequency than the Li-doped NKN ceramic. It is believed that the extrinsic contribution usually plays a very important role in the frequency-dependent piezoelectric property.<sup>43,44</sup> The extrinsic contribution to strains mainly comes from the domain switching, during which the ferroelectric materials change their spontaneously polarized states along the applied electric field direction. When the measuring frequency increases, the domain wall motion lags and then its contribution to the strain level also drops. The experimental results demonstrated that the domain wall motion in the  $x = 0.32$  sample is more flexible than that in Li-doped NKN, and is similar to that in soft PZT. As discussed above, this composition is an ergodic relaxor at room temperature, where the PNRs exist in a dynamic state with small size and meanwhile the thickness of domain walls (the regions where polarization is not well-defined) is comparable with the size of nanodomains.<sup>27</sup> Thus, upon the application of electric field, both the PNRs and domain walls would exhibit a fast response to the applied field and a full poling state could be obtained in the measuring frequency range, as proved by the almost unchanged values of  $P_{\max}$  and  $P_r$  [see Figs. 6(c) and (d)]. Nevertheless, it should be noted that there actually exists a very small decrease in  $P_{\max}$  as well as a slight increase in  $E_c$  with increasing frequency. This might be ascribed to the little contribution of domain wall movement similar to that observed in PZT 5H.<sup>45</sup> For the same reason, a slight decrease in the strain value with increasing frequency was still observed in Figs. 6(a) and (b). Moreover, it can be seen from Fig. 6(a) that the apparent  $S_{\text{obs}}$  values increased with increasing frequency, further confirming that the observed  $S_{\text{obs}}$  should be attributed to the hysteresis effect of the PNRs.

#### IV. Conclusions

BMT-PT- $x$ BNT ternary solid solution ceramics were manufactured by a solid-state reaction method. Their structure, dielectric behavior, and electric field-induced strain characteristics were specially investigated. A transformation from a diffuse-type-to-relaxor phase was observed owing to the change in domains from a frozen state to a dynamic state. The bipolar  $P$ - $E$  and  $S$ - $E$  loops and  $J$ - $E$  curves indicate that the electric field-induced strain was significantly enhanced by changing the BNT content, producing a peak value of  $\sim 0.41\%$  at a driving field of 7 kV/mm ( $d_{33}^*$  of  $\sim 590$  pm/V) at  $x = 0.32$ . This giant strain was mainly ascribed to the effect of the electric field-induced reversible ergodic relaxor-ferroelectric phase transition while the electrostriction and piezoelectric effect also made some contributions. Interestingly, this electric field-induced large strain showed a frequency insensitivity, which was ascribed to a fast response of both the PNRs and domain walls to the external electric field.

#### Acknowledgments

Financial support from the National Natural Science Foundation of China (grant nos. 51272060 and 51332002), the Natural Science Foundation Anhui Province (grant no. 1108085J14), and an opening fund of State Key Laboratory of New Ceramic and Fine Processing at Tsinghua University is gratefully acknowledged.

## References

- <sup>1</sup>J. F. Tressler, S. Alkoy, and R. E. Newnham, "Piezoelectric Sensors and Sensor Materials," *J. Electroceram.*, **2**, 257–72 (1998).
- <sup>2</sup>L. E. Cross, "Ferroelectric Materials for Electromechanical Transducer Applications," *Mater. Chem. Phys.*, **43**, 108–15 (1996).
- <sup>3</sup>G. H. Haertling, "Ferroelectric Ceramics: History and Technology," *J. Am. Ceram. Soc.*, **82** [4] 797–818 (1999).
- <sup>4</sup>K. Markowski, S. E. Park, S. Yoshikawa, and L. E. Cross, "Effect of Compositional Variations in the Lead Lanthanum Zirconate Stannate Titanate System on Electrical Properties," *J. Am. Ceram. Soc.*, **79** [12] 3297–304 (1996).
- <sup>5</sup>C. A. Randall, R. Eitel, B. Jones, T. R. Shrout, D. I. Woodward, and I. M. Reaney, "Investigation of a High  $T_c$  Piezoelectric System:  $(1-x)\text{Bi}(\text{Mg}_{1/2}\text{Ti}_{1/2})_2\text{O}_3\text{-xPbTiO}_3$ ," *J. Appl. Phys.*, **95** [7] 3633–9 (2004).
- <sup>6</sup>M. R. Suchomel and P. K. Davies, "Predicting the Position of the Morphotropic Phase Boundary in High Temperature  $\text{PbTiO}_3\text{-Bi(B'B')O}_3$  Based Dielectric Ceramics," *J. Appl. Phys.*, **96** [8] 4405–10 (2004).
- <sup>7</sup>J. Chen, X. L. Tan, W. Jo, and J. Rödel, "Temperature Dependence of Piezoelectric Properties of High- $T_c$   $\text{Bi}(\text{Mg}_{1/2}\text{Ti}_{1/2})_2\text{O}_3\text{-PbTiO}_3$ ," *J. Appl. Phys.*, **106** [3] 034109, 7pp (2009).
- <sup>8</sup>Q. Zhang, Z. R. Li, F. Li, Z. Xu, and X. Yao, "Temperature Dependence of Dielectric/Piezoelectric Properties of  $(1-x)\text{Bi}(\text{Mg}_{1/2}\text{Ti}_{1/2})_2\text{O}_3\text{-xPbTiO}_3$  Ceramics with an MPB Composition," *J. Am. Ceram. Soc.*, **93** [10] 3330–4 (2010).
- <sup>9</sup>S. J. Zhang, C. A. Randall, and T. R. Shrout, "High Curie Temperature Piezocrystals in the  $\text{BiScO}_3\text{-PbTiO}_3$  Perovskite System," *Appl. Phys. Lett.*, **83** [15] 3150–2 (2003).
- <sup>10</sup>M. R. Suchomel and P. K. Davies, "Enhanced Tetragonality in  $(x)\text{PbTiO}_3\text{-}(1-x)\text{Bi}(\text{Zn}_{1/2}\text{Ti}_{1/2})_2\text{O}_3$  and Related Solid Solution Systems," *Appl. Phys. Lett.*, **86** [26] 262905, 3pp (2005).
- <sup>11</sup>I. Grinberg, M. R. Suchomel, P. K. Davies, and A. M. Rappe, "Predicting Morphotropic Phase Boundary Locations and Transition Temperatures in Pb- and Bi-Based Perovskite Solid Solutions from Crystal Chemical Data and First-Principles Calculations," *J. Appl. Phys.*, **98** [9] 094111, 10pp (2005).
- <sup>12</sup>A. Dwivedi, C. A. Randall, and G. A. Rossetti, "Thermal History Induced Variable Relaxor Behavior in the High  $T_c$  Ternary Ferroelectric  $0.6\text{Bi}(\text{Mg}_{1/2}\text{Ti}_{1/2})_2\text{O}_3\text{-}0.05\text{Bi}(\text{Zn}_{1/2}\text{Ti}_{1/2})_2\text{O}_3\text{-}0.35\text{PbTiO}_3$ ," *Mater. Lett.*, **65**, 3034–6 (2011).
- <sup>13</sup>A. Dwivedi, W. G. Qu, and C. A. Randall, "Preparation and Characterization of High-Temperature Ferroelectric  $x\text{Bi}(\text{Mg}_{1/2}\text{Ti}_{1/2})_2\text{O}_3\text{-yBi}(\text{Zn}_{1/2}\text{Ti}_{1/2})_2\text{O}_3\text{-zPbTiO}_3$  Perovskite Ternary Solid Solution," *J. Am. Ceram. Soc.*, **94** [12] 4371–5 (2011).
- <sup>14</sup>R. Rai, A. Kholkin, S. Pandey, and N. K. Singh, "Investigation of Structural, Electrical and Magnetic Properties of  $\text{BiFeO}_3\text{-Bi}(\text{MgTi})_2\text{O}_3\text{-PbTiO}_3$  Ceramic System," *J. Alloy. Compd.*, **488** [1] 459–64 (2009).
- <sup>15</sup>R. Rai, A. L. Kholkin, and S. Sharma, "Multiferroic Properties of  $\text{BiFeO}_3$  Doped  $\text{Bi}(\text{MgTi})_2\text{O}_3\text{-PbTiO}_3$  Ceramic System," *J. Alloy. Compd.*, **506** [2] 815–9 (2010).
- <sup>16</sup>L. L. Fan, J. Chen, H. J. Kang, L. J. Liu, L. Fang, J. X. Deng, R. B. Yu, and X. R. Xing, "Structure, Piezoelectric, and Ferroelectric Properties of  $\text{BaZrO}_3$  Substituted  $\text{Bi}(\text{Mg}_{1/2}\text{Ti}_{1/2})_2\text{O}_3\text{-PbTiO}_3$  Perovskite," *J. Appl. Phys.*, **111** [10] 104118, 6pp (2012).
- <sup>17</sup>J. Chen, J. Y. Li, L. L. Fan, N. Zou, P. F. Ji, L. J. Liu, L. Fang, H. J. Kang, and X. R. Xing, "Enhanced Piezoelectric and Antiferroelectric Properties of High- $T_c$  Perovskite of Zr-Substituted  $\text{Bi}(\text{Mg}_{1/2}\text{Ti}_{1/2})_2\text{O}_3\text{-PbTiO}_3$ ," *J. Appl. Phys.*, **112** [7] 074101, 6pp (2012).
- <sup>18</sup>D. D. Khalyavin, A. N. Salak, N. P. Vyshatko, A. B. Lopes, N. M. Olekhovich, A. V. Pushkarev, I. I. Maroz, and Y. V. Radyush, "Crystal Structure of Metastable Perovskite  $\text{Bi}(\text{Mg}_{1/2}\text{Ti}_{1/2})_2\text{O}_3$ : Bi-Based Structural Analogue of Antiferroelectric  $\text{PbZrO}_3$ ," *Chem. Mater.*, **18** [21] 5104–10 (2006).
- <sup>19</sup>J. Fu and R. Z. Zuo, "Giant Electrostrains Accompanying the Evolution of a Relaxor Behavior in  $\text{Bi}(\text{Mg,Ti})_2\text{O}_3\text{-PbZrO}_3\text{-PbTiO}_3$  Ferroelectric Ceramics," *Acta Mater.*, **61**, 3687–94 (2013).
- <sup>20</sup>S. T. Zhang, A. B. Kounga, E. Aulbach, H. Ehrenberg, and J. Rödel, "Giant Strain in Lead-Free Piezoceramics  $\text{Bi}_{0.5}\text{Na}_{0.5}\text{TiO}_3\text{-BaTiO}_3\text{-K}_{0.5}\text{Na}_{0.5}\text{NbO}_3$  System," *Appl. Phys. Lett.*, **91** [11] 112906, 3pp (2007).
- <sup>21</sup>W. Jo, T. Granzow, E. Aulbach, J. Rödel, and D. Damjanovic, "Origin of the Large Strain Response in  $(\text{K}_{0.5}\text{Na}_{0.5})\text{NbO}_3$ -Modified  $(\text{Bi}_{0.5}\text{Na}_{0.5})\text{TiO}_3\text{-BaTiO}_3$  Lead-Free Piezoceramics," *J. Appl. Phys.*, **105** [9] 094102, 5pp (2009).
- <sup>22</sup>K. Wang, A. Hussain, W. Jo, and J. Rödel, "Temperature-Dependent Properties of  $(\text{Bi}_{1/2}\text{Na}_{1/2})\text{TiO}_3\text{-}(\text{Bi}_{1/2}\text{K}_{1/2})\text{TiO}_3\text{-SrTiO}_3$  Lead-Free Piezoceramics," *J. Am. Ceram. Soc.*, **95** [7] 2241–7 (2012).
- <sup>23</sup>A. Hussain, C. W. Ahn, J. S. Lee, A. Ullah, and I. W. Kim, "Large Electric-Field-Induced Strain in Zr-Modified Lead-Free  $\text{Bi}_{0.5}(\text{Na}_{0.78}\text{K}_{0.22})_{0.5}\text{TiO}_3$  Piezoelectric Ceramics," *Sensor Actuat A-Phys.*, **158**, 84–9 (2010).
- <sup>24</sup>W. Jo, R. Dittmer, M. Acosta, J. D. Zang, C. Groh, E. Sapper, K. Wang, and J. Rödel, "Giant Electric-Field-Induced Strains in Lead-Free Ceramics for Actuator Applications-Status and Perspective," *J. Electroceram.*, **29** [1] 71–93 (2012).
- <sup>25</sup>L. E. Cross, "Relaxor Ferroelectrics," *Ferroelectrics*, **76**, 241–67 (1987).
- <sup>26</sup>V. Westphal, W. Kleemann, and M. D. Glinchuk, "Diffuse Phase Transitions and Random-Field-Induced Domain States of the 'Relaxor' Ferroelectric  $\text{PbMg}_{1/3}\text{Nb}_{2/3}\text{O}_3$ ," *Phys. Rev. Lett.*, **68** [6] 847–50 (1992).
- <sup>27</sup>A. A. Bokov and Z. G. Ye, "Recent Progress in Relaxor Ferroelectrics with Perovskite Structure," *J. Mater. Sci.*, **41**, 31–52 (2006).
- <sup>28</sup>V. V. Shvartsman, W. Kleemann, J. Dec, Z. K. Xu, and S. G. Lu, "Diffuse Phase Transition in  $\text{BaTi}_{1-x}\text{Sn}_x\text{O}_3$  Ceramics: An Intermediate State Between Ferroelectric and Relaxor Behavior," *J. Appl. Phys.*, **99** [12] 124111, 8pp (2006).
- <sup>29</sup>X. Y. Wei, Y. J. Feng, and X. Yao, "Dielectric Relaxation Behavior in Barium Titanate Ferroelectric Ceramics with Diffused Phase Transition," *Appl. Phys. Lett.*, **83** [10] 2031–3 (2007).
- <sup>30</sup>J. Kreisel, A. M. Glazer, P. Bouvier, and G. Lucazeau, "High-Pressure Raman Study of a Relaxor Ferroelectric: The  $\text{Na}_{0.5}\text{Bi}_{0.5}\text{TiO}_3$  Perovskite," *Phys. Rev. B*, **63** [17] 174106, 10pp (2001).
- <sup>31</sup>M. Gröting, I. Kornev, B. Dkhil, and K. Albe, "Pressure-Induced Phase Transitions and Structure of Chemically Ordered Nanoregions in the Lead-Free Relaxor Ferroelectric  $\text{Na}_{1/2}\text{Bi}_{1/2}\text{TiO}_3$ ," *Phys. Rev. B*, **86** [13] 134118, 10pp (2012).
- <sup>32</sup>M. K. Niranjana, T. Karthik, S. Asthana, J. Pan, and U. V. Waghmare, "Theoretical and Experimental Investigation of Raman Modes, Ferroelectric and Dielectric Properties of Relaxor  $\text{Na}_{0.5}\text{Bi}_{0.5}\text{TiO}_3$ ," *J. Appl. Phys.*, **113** [19] 194106, 7pp (2013).
- <sup>33</sup>R. D. Shannon, "Revised Effective Ionic Radii and Systematic Studies of Interatomic Distances in Halides and Chalcogenides," *Acta Cryst.*, **32**, 751–67 (1976).
- <sup>34</sup>K. Uchino and S. Nomura, "Critical Exponents of the Dielectric Constants in Diffused-Phase-Transition Crystals," *Ferroelectr. Lett.*, **44** [1] 55–61 (1982).
- <sup>35</sup>W. Chen, X. Yao, and X. Y. Wei, "Tunability and Ferroelectric Relaxor Properties of Bismuth Strontium Titanate Ceramics," *Appl. Phys. Lett.*, **90** [18] 182902, 3pp (2007).
- <sup>36</sup>Y. Liu, R. L. Withers, B. Nguyen, and K. Elliott, "Structurally Frustrated Polar Nanoregions in  $\text{BaTiO}_3$ -Based Relaxor Ferroelectric Systems," *Appl. Phys. Lett.*, **91** [15] 152907, 3pp (2007).
- <sup>37</sup>C. Laulhé, F. Hippert, J. Kreisel, M. Maglione, A. Simon, J. L. Hazemann, and V. Nassif, "EXAFS Study of Lead-Free Relaxor Ferroelectric  $\text{BaTi}_{1-x}\text{Zr}_x\text{O}_3$  at the Zr K Edge," *Phys. Rev. B*, **74** [1] 014106, 12pp (2006).
- <sup>38</sup>V. V. Shvartsman and D. C. Lupascu, "Lead-Free Relaxor Ferroelectrics," *J. Am. Ceram. Soc.*, **95** [1] 1–26 (2012).
- <sup>39</sup>A. A. Bokov, "Ferroelectric Domains and Polar Clusters in Disordered Structures," *Ferroelectrics*, **190**, 197–202 (1997).
- <sup>40</sup>M. D. Glinchuk and R. Farhi, "A Random Field Theory Based Model for Ferroelectric Relaxors," *J. Phys.: Condens. Matter*, **8**, 6985–96 (1996).
- <sup>41</sup>G. Viola, H. P. Ning, X. J. Wei, M. Deluca, A. Adomkevicius, J. Khaliq, M. J. Reece, and H. X. Yan, "Dielectric Relaxation, Lattice Dynamics and Polarization Mechanisms in  $\text{Bi}_{0.5}\text{Na}_{0.5}\text{TiO}_3$ -Based Lead-Free Ceramics," *J. Appl. Phys.*, **114** [1] 014107, 9pp (2013).
- <sup>42</sup>J. Zhou, K. Wang, F. Li, J. F. Li, X. W. Zhang, and Q. M. Wang, "High and Frequency-Insensitive Converse Piezoelectric Coefficient Obtained in  $\text{AgSbO}_3$ -Modified  $(\text{Li, K, Na})(\text{Nb, Ta})\text{O}_3$  Lead-Free Piezoceramics," *J. Am. Ceram. Soc.*, **96** [2] 519–23 (2013).
- <sup>43</sup>D. Damjanovic, "Logarithmic Frequency Dependence of the Piezoelectric Effect due to Pinning of Ferroelectric-Ferroelastic Domain Walls," *Phys. Rev. B*, **55** [2] 649–52 (1997).
- <sup>44</sup>A. J. Masys, W. Ren, G. Yang, and B. K. Mukherjee, "Piezoelectric Strain in Lead Zirconate Titanate Ceramics as a Function of Electric Field, Frequency, and dc Bias," *J. Appl. Phys.*, **94** [2] 1155–62 (2003).
- <sup>45</sup>K. B. Chong, F. Guiu, and M. J. Reece, "Thermal Activation of Ferroelectric Switching," *J. Appl. Phys.*, **103** [1] 014101, 7pp (2008). □